X-ray scattering measurements of particle orientation in a sheared polymer/clay dispersion

Saswati Pujari, Leah Dougherty, Christophe Mobuchon, Pierre Carreau, Marie-Claude Heuzey, Wesley R Burghardt

HAL Id: hal-01007437

https://hal.science/hal-01007437

Submitted on 21 Oct 2017

X-ray scattering measurements of particle orientation in a sheared polymer/clay dispersion

**Saswati Pujari · Leah Dougherty ·
Christophe Mobuchon · Pierre J. Carreau ·
Marie-Claude Heuzey · Wesley R. Burghardt**

Abstract We report steady and transient measurements of particle orientation in a clay dispersion subjected to shear flow. An organically modified clay is dispersed in a Newtonian polymer matrix at a volume fraction of 0.02, using methods previously reported by Mobuchon et al. (Rheol Acta 46: 1045, 2007). In accord with prior studies, mechanical rheometry shows yield stress-like behavior in steady shear, while time dependent growth of modulus is observed following flow cessation. Measurements of flow-induced orientation in the flow-gradient plane of simple shear flow using small-angle and wide-angle X-ray scattering (SAXS and WAXS) are reported. Both SAXS and WAXS reveal increasing particle orientation as shear rate is increased. Partial relaxation of nanoparticle orientation upon flow cessation is well correlated with time-dependent changes in complex modulus. SAXS and WAXS data provide qualitatively similar results; however, some quantitative differences are attributed to differences in the length scales probed by these techniques.

S. Pujari · L. Dougherty · W. R. Burghardt (✉)
Department of Chemical and Biological Engineering,
Northwestern University, Evanston, IL, 60208, USA
e-mail: w-burghardt@northwestern.edu

W. R. Burghardt
Department of Material Science and Engineering,
Northwestern University, Evanston, IL, 60208 USA

C. Mobuchon · P. J. Carreau · M.-C. Heuzey
Chemical Engineering Department, Center for Applied
Research on Polymers and Composites (CREPEC),
Ecole Polytechnique, Montreal, QC, Canada H3C3A7

Introduction

The addition of layered silicates to polymers is an important method to produce new and improved materials. Relative to neat polymers, clay nanocomposites have shown enhanced mechanical and flame retardant properties, increased dimensional stability, and reduced permeability (Kojima et al. 1993; Giannelis 1996; Fornes et al. 2001; Nam et al. 2001). A variety of polymer matrices, including polyamides, polystyrene, and polypropylene, have been used to produce clay nanocomposites (Okada et al. 1987; Giannelis et al. 1999; Alexandre and Dubois 2000; Fornes et al. 2001). In all nanocomposites, achieving the desired property improvements requires understanding and control of the structure of the dispersed clay particles. Nanocomposite properties will depend critically on two aspects of structure: the relative position of the clay particles with respect to each other (especially the degree of exfoliation of individual nanoscale clay sheets) and the orientation distribution of the dispersed clay particles. Thermodynamics is expected to play a central role in determining the equilibrium state of dispersion (Balazs 2003); however, flow fields during processing—either in nanocomposite preparation, or production of final products—will also significantly influence the nanocomposite structure. Thus, to design nanocomposites with stable dispersed states and desired final properties, it is important to study structural changes taking place during flow.

Rheology is an important tool for interrogating flow-induced structural changes in polymer nanocomposites

(Vermant et al. 2007). Many researchers have reported rheological phenomena such as the emergence of a solid-like low frequency shear modulus (Galgali et al. 2001; Krishnamoorti and Yurekli 2001; Solomon et al. 2001; Aubry et al. 2005; Xu et al. 2005) and nonlinear behavior in transient flow conditions (Lim and Park 2001; Solomon et al. 2001; Koo et al. 2003; Ren and Krishnamoorti 2003; Mobuchon et al. 2007). Both linear and nonlinear rheology are sensitive to microstructural changes, and each provides a means to study the structural state of clay nanocomposites in the melt state. However, the observed rheological behavior may be influenced by several factors, such as particle orientation induced by the external flow field, interparticle interactions and associated formation of percolated network structures, and possible direct coupling between polymer and particle dynamics. Such complexity places limitations on rheology—by itself—as a structural characterization tool.

Kinetics of structural relaxation in clay nanocomposites have been studied by Ren and Krishnamoorti (2003) using linear viscoelastic measurements. These studies found that the increase in storage modulus was independent of the nanoparticle size, temperature and viscosity of the polymeric matrix, leading to the conclusion that, in the system studied, the underlying structural changes were not a consequence of Brownian randomization. Solomon et al. (2001) observed that stress overshoots following reversal of steady shear flow were dependent on the rest time before reversal. The magnitude of the overshoot increased with increasing rest time, but over time scales much shorter than that expected for Brownian rotation in such systems. Solomon et al. (2001) thus concluded that the reorientation of structure was due to attractive interactions between the clay platelets and not due to Brownian motion. Lele et al. (2002) reported relaxation of orientation after steady pre-shearing using both rheology and in situ X-ray diffraction. The time scales for relaxation were found to be shorter than the time scale required for Brownian relaxation. However, since they found that an uncompatibilized clay dispersion showed slower relaxation than a compatibilized system, they ruled out the possibility that attractive interactions promote relaxation. X-ray scattering has been used by several researchers to characterize orientation in sheared or processed clay nanocomposites (Varlot et al. 2001; Bafna et al. 2003; Galgali et al. 2004). However, most studies have involved ex situ measurements on the final orientation in the solid state. While limited in situ data are available (Medellin-Rodriguez et al. 2001; Lele et al. 2002; Camerel et al. 2003), there is still a paucity of time-resolved orientation data in transient flows.

Mobuchon et al. (2007) performed an extensive rheological characterization of a clay dispersion in a Newtonian polybutene matrix, yielding a partially dispersed, intercalated suspension. Since the matrix was rheologically uninteresting, the non-Newtonian rheology of the suspension could be directly attributed to the dispersed clay nanoparticles. Both linear and nonlinear rheological testing were used to probe the effects of flow history on rheology. Linear viscoelastic measurements following cessation of shear flow revealed that (1) the complex modulus observed immediately upon flow cessation depended on the prior shear rate; (2) the complex modulus evolved over an extended period during relaxation; and (3) the final complex modulus also depended on the previous shear rate. The particles used for this study were Brownian, providing a logical explanation for structural relaxation after shear cessation. The existence of shear history-dependent equilibrium states (attributed to the formation of different final structural states of the clay particles) was argued to be due to the large hydrodynamic forces required to overcome the effects of the excluded volume of the clay particles, hence restricting the Brownian mobility of clay particles due to "lack of space." At the same time, transient experiments such as flow reversal and step down suggested that a single unique structural steady state is associated with each shear rate, although thixotropic responses meant that some amount of shearing was required to reach that state.

As illustrated by the above discussion, rheological data on polymer nanocomposites are often interpreted in terms of two distinct structural characteristics: the orientation distribution of the individual clay particles, and particle "network" structures, mediated by interparticle interactions; indeed, attempts have been made to model both types of structure to provide insights into the interpretation of transient rheological phenomena (Letwimolnun et al. 2007). Mobuchon et al. (2007) have previously coordinated rheological studies with rheo-optical investigations using light scattering and dichroism (Mobuchon et al. 2009a), and real-space imaging using confocal microscopy (Mobuchon et al. 2009b) under shear; these techniques intrinsically probe relatively large length scales. In this work, X-ray scattering is used to directly measure the degree of *particle orientation* in both steady and time dependent shear flows; our goal is to directly interrogate the extent to which bulk rheology is correlated with local particle orientation. Both wide-angle and small-angle X-ray scattering are used

to probe orientation. Since it relies on diffraction from the layered internal structure of individual clay tactoids, wide angle X-ray scattering (WAXS) provides a robust and reliable representation of the particle orientation distribution. In principle, anisotropic small-angle X-ray scattering (SAXS), arising from the overall anisotropic disk-like shape of clay particles, should yield equivalent information. However, the propensity for formation of interparticle clusters or networks on larger length scales in clay dispersions (Pignon et al. 1997, 1998; Schaeffer and Justice 2007) may be manifested in SAXS data; indeed it will be shown that SAXS and WAXS data provide somewhat different perspectives on the flow induced orientation state.

Experimental methods

The layered silicate used to prepare the model suspension was an organically modified montmorillonite, clay (Cloisite 15A, Southern Clay Products). The nonpolar Newtonian dispersing matrix was a blend of polybutenes (Indopol, BP), with a viscosity of 28.5 Pa s at 25°C. All measurements reported here were conducted on a sample with a 0.02 volume fraction of clay. The sample preparation protocols are identical to those reported by Mobuchon et al. (2007); however, this sample is lower in volume fraction. Nevertheless, the rheological data reported below are very similar to those reported by Mobuchon et al. (2007). Using an estimated average particle diameter of 320 nm (Mobuchon et al. 2007), the rotational diffusivity $\left(D_r = 3k_B T \big/ 4\eta d^3 \right)$ of the clay particles is calculated to be 0.0033 s^{-1}. TEM imaging of similar samples (Mobuchon et al. 2007), and the presence of strong diffraction peaks in WAXS data presented below indicate that complete exfoliation of individual clay sheets is not achieved. Rather, the clay particles consist of layered "tactoids."

Rheological testing was carried out using a strain controlled rheometer (ARES, Rheometric Scientific). All tests were conducted at room temperature using 50 mm cone and plate fixtures with a cone angle of 0.04 rad. To maintain a consistent shear history at the beginning of each measurement, the suspension was subjected to pre-shearing at 25 s^{-1} for 120 s. This protocol was adopted directly from Mobuchon et al. (2007).

SAXS studies were performed using synchrotron radiation at beam line 5ID-D of the Advanced Photon Source (APS) at the Argonne National Lab. Highly collimated X-rays with energy of 15 keV were se-lected from an undulator beam using a double crystal monochromator. To study particle orientation in the 1–2 (flow-gradient) plane, the sample was sheared using a custom designed annular cone and plate shear cell (Caputo and Burghardt 2001). The high energy used in these experiments reduces absorption due to the sample thickness (~1 cm) in this shear cell. Two-dimensional (2D) scattering patterns were collected using a CCD detector (MarCCD) at rates of up to 0.25 frames/s, with a 9-m sample to detector distance. WAXS studies were conducted using the same shear cell, at APS beam line 5BM-D. Here, a focused bending magnet X-ray beam was passed through a double crystal monochromator to provide energy of 20 keV. The sample to detector distance in WAXS experiments was 73 cm, and scattering patterns were collected using a similar 2D detector at rates of up to 0.4 frames/s. In addition to reducing absorption, the use of high X-ray energy has the beneficial effect of shifting diffraction to smaller angles, allowing the WAXS feature of interest to cleanly exit the shear cell. All scattering patterns are automatically corrected for background electronic noise. In both SAXS and WAXS experiments, vacuum tanks were placed between the shear cell and the detector to minimize background air scattering. Since homogenous polymer melts are expected to scatter negligibly at the low scattering angles used here (save for density fluctuations associated with compressibility), both wide- and small-angle scattering should be dominated by the dispersed particles. Thus, no further baseline subtraction was attempted.

The cone and plate shear cell used for X-ray experiments has a wide cone angle (5°), and the sample has a free surface at its outer edge. Experience has shown that high shear rates can cause expulsion of viscoelastic samples from the test fixtures. The prolonged high shear rate pre-shearing protocol was thus avoided in the X-ray experiments. We have nevertheless found that orientation data are quite reproducible, provided the sample is sheared sufficiently long at the desired shear rate (in the end, this precaution appears not to have been necessary, as WAXS experiments— performed some time after the SAXS experiments— were ultimately extended to shear rates as high as 100 s^{-1} without sample expulsion).

Anisotropic X-ray scattering from dispersions of layered clays offers two possible avenues for probing the particle orientation state. In reciprocal space, wide-angle diffraction from the internal layered structure of each individual clay particle is slaved to that particle's orientation, providing a direct mapping of the

particle orientation distribution function to anisotropic azimuthal intensity distributions in WAXS patterns. On the other hand, small-angle scattering probes length scales commensurate with the macroscopic dimensions of clay particles (tens of nanometers in thickness; hundreds of nanometers in diameter). Any flow-induced particle orientation should also be manifested in anisotropic scattering in the SAXS regime, as well. Thus, SAXS and WAXS can provide complimentary probes of particle orientation in sheared suspensions, at different length scales.

A sample with perfectly aligned disk-like particles would exhibit a 2D SAXS pattern with a sharp streak of scattered intensity along the direction normal to the particles' flat surfaces. Similarly, in the WAXS regime, a 2D pattern would show sharp diffraction spots along the particle normals. Decreasing degrees of alignment would lead to azimuthal broadening of each of these features, ultimately yielding, for a randomly oriented sample, an isotropic blob-like feature in 2D SAXS, and an isotropic diffraction ring in 2D WAXS. In 2D small angle scattering (and even in the 'wide angle' measurements reported here, for which the scattering angle of the diffraction feature of interest is just $1.18°$ owing to the high energy), a 'slice' of reciprocal space, roughly perpendicular to the incident beam, is sampled. In this geometry, only those particles whose normal vectors lie within this slice will contribute to observable scattering. In this work, therefore, scattering measurements sample the orientation distribution function of those particles whose normals lie within the 1–2 plane. Dilute solution hydrodynamics of thin disk-like particles shows that as particles execute Jeffery orbits (Jeffery 1922), they spend the majority of their time 'lying down flat' in shear flow, with normals tending to accumulate along the velocity gradient direction. Thus, the sampling of reciprocal space employed here is best suited for probing flow-induced orientation, and facilitates measurements of both the degree and direction of particle alignment in the 1–2 plane.

A quantitative measure of the shear-induced anisotropy in each SAXS pattern was obtained by calculating a second moment tensor of the scattering vector $\mathbf{q}$ weighted by the scattering intensity $I(\mathbf{q})$, an approach introduced by Salem and Fuller (1985). In the 1–2 plane of shear flow, the second moment tensor is defined by:

$$\langle \mathbf{qq} \rangle = \begin{pmatrix} \langle q_1 q_1 \rangle & \langle q_1 q_2 \rangle \\ \langle q_1 q_2 \rangle & \langle q_2 q_2 \rangle \end{pmatrix} = \frac{\iint \mathbf{qq} I(\mathbf{q}) \, dq_1 dq_2}{\iint q^2 I(\mathbf{q}) \, dq_1 dq_2}, \tag{1}$$

where 1 and 2 designate the flow and velocity gradient directions, respectively. The normalization by the total scattering intensity in Eq. 1 eliminates effects due to fluctuations in the incident beam intensity. The degree of anisotropy in each scattering pattern may be quantified by an "anisotropy factor" (AF), computed as the difference in the principal values of $\langle \mathbf{qq} \rangle$, while the orientation angle relative to the flow direction (χ) is determined from the principal directions of $\langle \mathbf{qq} \rangle$:

$$AF = \sqrt{(\langle q_1 q_1 \rangle - \langle q_2 q_2 \rangle)^2 + 4 \langle q_1 q_2 \rangle^2}, \tag{2}$$

$$\chi = \frac{1}{2} \tan^{-1} \left(\frac{2 \langle q_1 q_2 \rangle}{\langle q_1 q_1 \rangle - \langle q_2 q_2 \rangle} \right). \tag{3}$$

Defined in this way, AF ranges from 0 to 1 for random and perfect alignment, respectively. Thus, it is functionally similar to the Hermann's order parameter ($\langle P_2 \rangle$) frequently used to quantify alignment in oriented polymer materials. Methods for computing $\langle P_2 \rangle$ from 2D X-ray scattering images require an assumption that the underlying orientation state is uniaxially symmetric, an assumption that is generally false in shear flow. The second moment tensor approach used here neither requires nor imposes prior assumptions about symmetry of the orientation state, while providing a direct and quantitative representation of the degree and direction of anisotropy present in the scattering pattern. This method of quantifying anisotropy and orientation angle from SAXS patterns has been used for other systems like bicontinuous microemulsions (Caputo et al. 2002) and carbon nanotube suspensions (Pujari et al. 2009).

A similar analysis may be applied to WAXS patterns, for which a convenient starting point is an azimuthal intensity distribution, $I(\theta)$, extracted from each 2D scattering pattern over a radial range encompassing the layer diffraction peak (Fig. 1f). The azimuthal angle, θ, is measured away from the flow direction towards the gradient direction. Each point on an azimuthal scan is represented by a unit vector $\mathbf{u}$. A second moment tensor of this vector, weighted by the scattered intensity, is then defined as:

$$\langle \mathbf{uu} \rangle = \begin{bmatrix} \langle u_1 u_1 \rangle & \langle u_1 u_2 \rangle \\ \langle u_1 u_2 \rangle & \langle u_2 u_2 \rangle \end{bmatrix} = \frac{\int \mathbf{uu} I(\theta) \, d\theta}{\int I(\theta) \, d\theta}, \tag{4}$$

where 1 and 2 designate the flow and velocity gradient directions, respectively. The degree of anisotropy in each scattering pattern is, again, quantified by an anisotropy factor (AF), computed in this case as the difference in the principal values of $\langle \mathbf{uu} \rangle$, while the

Fig. 1 Two-dimensional scattering images measured in the 1–2 plane for the 2.0 vol.% clay dispersion during shear: SAXS patterns collected at shear rates of **a** 0.07, **b** 0.7, and **c** 7.0 s^{-1}; and WAXS patterns collected at shear rates of **d** 0.1, **e** 1.0, and **f** 10 s^{-1}. The scattering peak in the WAXS images is located at $q = 2.1$ nm^{-1}, corresponding to a layer spacing of 3 nm. *Dashed lines* in (**f**) indicate the radial range over which the WAXS peak is integrated when computing azimuthal intensity scans, $I(\theta)$
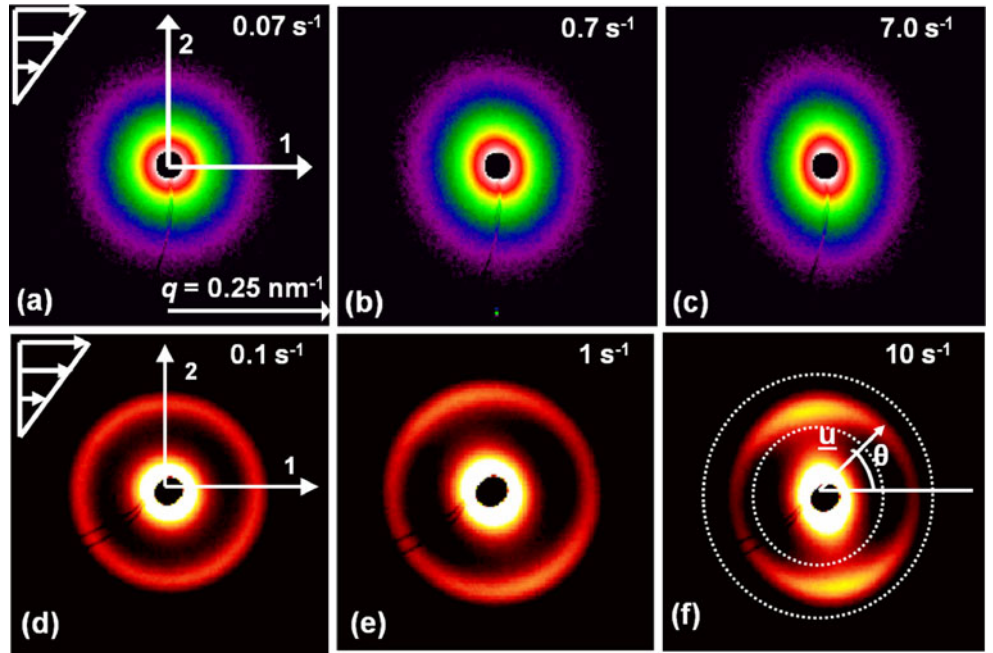
orientation angle relative to the flow direction (χ) is determined from the principal directions of $\langle \mathbf{uu} \rangle$:

$$\text{AF} = \sqrt{(\langle u_1 u_1 \rangle - \langle u_2 u_2 \rangle)^2 + 4\langle u_1 u_2 \rangle^2}, \quad (5)$$

$$\chi = \frac{1}{2} \tan^{-1} \left(\frac{2\langle u_1 u_2 \rangle}{\langle u_1 u_1 \rangle - \langle u_2 u_2 \rangle} \right). \quad (6)$$

The analysis methods represented by Eqs. 1–6 are closely related. In fact, Eqs. 4–6 follow directly from Eqs. 1–3 for the case in which scattered intensity is concentrated in a peak at a single value of q. In either regime, a (hypothetical) case of perfect alignment would lead to concentration of all scattered intensity along the direction of the particle normals, resulting in AF = 1. As a result, it is anticipated that SAXS and WAXS should yield similar measures of anisotropy.

Results and discussion

Both SAXS and WAXS patterns reveal that clay particles become progressively aligned with increasing shear rate (Fig. 1). SAXS shows a nearly isotropic "blob" of scattering at low shear rates (Fig. 1a), indicative of nearly random orientation. As shear rate increases, the SAXS feature becomes increasingly anisotropic (Fig. 1b, c). Recalling that scattering from disk-like particles is concentrated normal to their long axis, the

higher intensity observed along the gradient axis in these images corresponds to a preferred orientation of the clay particles' long axes towards the flow direction. It can also be readily observed that the direction of the most intense scattering in these patterns is not simply aligned along the gradient direction but is rotated somewhat counter clockwise. Correspondingly, this means that the average particle orientation direction is rotated away from the flow direction. As shear rate increases, the direction of the most intense scattering rotates closer to the gradient direction, indicating particle orientation closer to the flow direction. Similar features are also seen in WAXS patterns (Fig. 1d–f), where a nearly isotropic ring of scattered intensity at low rates gives way to peaks that both increase in magnitude and rotate progressively towards the gradient direction as shear rate increases. Again, since wide-angle diffraction from the layered disk-like clay particles is confined along the particle normals, these patterns indicate increasing degrees of particle alignment towards the flow direction with increasing shear rate. The WAXS patterns also reveal anisotropic scattering at smaller q values; this is simply the wide-angle limit of the SAXS feature in Fig. 1a–c. All SAXS-derived calculations of anisotropy reported here are derived from the dedicated SAXS experiments. However, calculations of anisotropy and orientation angle from the limited SAXS data in the small q regime of the WAXS images yield similar results.

The first order diffraction feature observed in WAXS patterns is unambiguously associated with the internal layering of clay tactoids. To better define the structural length scales being probed in the SAXS data, Fig. 2 compares azimuthally integrated $I(q)$ data to representative theoretical calculations of the single-particle form factor, $P(q)$, for randomly oriented disks of radius R and thickness t (Guinier and Fournet 1955):

$$P(q) = 4 \int_0^1 \left(\frac{J_1\left(qR\sqrt{1-x^2}\right)}{qR\sqrt{1-x^2}} \right)^2 \left(\frac{\sin\left(qtx/2\right)}{qtx/2} \right)^2 dx. \tag{7}$$

In the limit $t \to 0$, $P(q)$ is given by the simpler expression (Guinier and Fournet 1955):

$$P(q) = \frac{2}{q^2 R^2} \left[1 - \frac{J_1(2qR)}{qR} \right]. \tag{8}$$

Intraparticle interference begins to suppress scattered intensity in thin disks when $qR \sim O(1)$, the Guinier regime. For $qR >> 1$, Eq. 8 predicts the characteristic q^{-2} power law associated with random thin disks. Accounting for finite disk thickness, Eq. 7 predicts a pseudo q^{-2} power law for $1/R < q < 1/t$ (here we assume $R > t$). For $q > 1/t$, scattered intensity drops off more rapidly and, for monodisperse thickness, exhibits

well-defined diffraction "fringes." In the presence of a distribution of thicknesses, these fringes would be smeared out, and the $q \sim 1/t$ region would instead be characterized by a transition from a q^{-2} power law to a q^{-4} power law (the Porod regime).

Since Eqs. 7 and 8 assume a random orientation distribution, the data selected for Fig. 2 were obtained at a low shear rate; results presented below (Fig. 4) show the sample to be nearly isotropic under these conditions, at least within the 1–2 plane. Spanning a q-range of 0.02 to 0.25 nm^{-1}, our SAXS experiments probe structure on roughly 4 to 50 nm length scales, commensurate with the range of tactoid thicknesses observed by TEM of similar organoclay/polybutene dispersions by Mobuchon et al. (2007). Thus, while SAXS inherently probes larger length scales than WAXS, under the conditions used here, SAXS data still reflect anisotropy in structure at the single-particle length scale, reinforcing the expectation that SAXS and WAXS may provide similar insights into flow-induced particle orientation. In particular, note that even the average particle radius of 160 nm is too large to be resolved in these SAXS experiments. The observed $I(q)$ is rather featureless over the accessible q-range, exhibiting roughly a power-law with slope $= -2.7$, which can be interpreted as the predicted crossover between slopes of -2 (disk) and -4 (Porod), broadened by polydispersity in tactoid thickness.

Steady shear rheology of this 2 vol.% dispersion shows behavior very similar to that observed by Mobuchon et al. (2007) in the analogous 4 vol.% dispersion, approaching a yield stress behavior at low rates
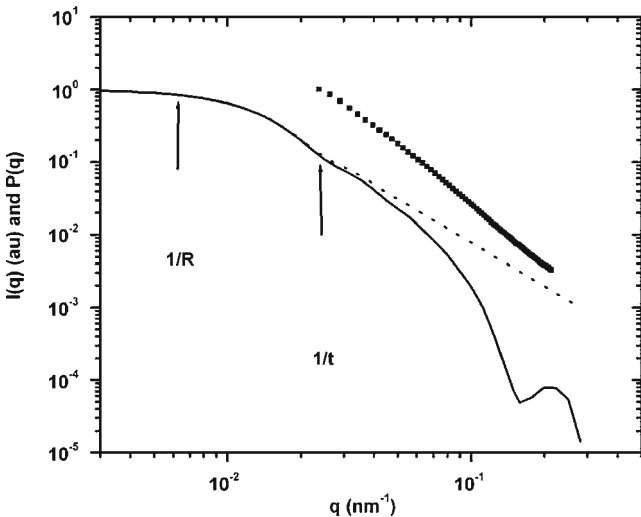
Fig. 2 Azimuthally averaged small-angle X-ray scattering data, $I(q)$, collected during shear at a rate of 0.02 s^{-1} (symbols), compared with form factor, $P(q)$, computed for randomly oriented disks using representative values of radius $R = 160$ nm, and thickness $t = 40$ nm (solid line, Eq. 7) and in limit of zero thickness (dashed line, Eq. 8)
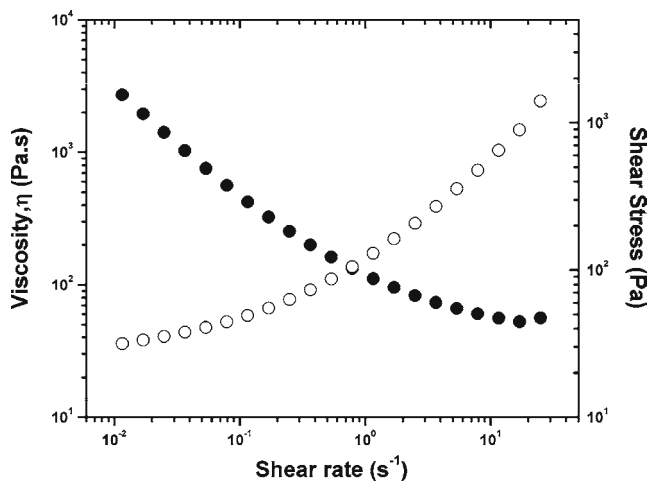
Fig. 3 Steady shear viscosity (filled circles) and shear stress (unfilled circles) measured as a function of shear rate for the 2 vol.% clay dispersion

and a viscosity plateau at high rates (Fig. 3). The yield stress at low rates is attributed to the solid-like properties of a particulate network. When the suspension is sheared at high rates, this network structure is broken down and the measured viscosity measured drops close to the matrix viscosity (28.5 Pa s in this sample).

Direct insights into the shear-rate dependent structural state are obtained from corresponding steady state X-ray scattering measurements (Fig. 4). In both SAXS and WAXS experiments, time resolved measurements of orientation were performed in series of experiments including inception, reversal and step changes at various shear rates. The steady state anisotropy and orientation angle were calculated by averaging values after prolonged shearing (at least 30 strain units). Error bars indicate the variability in anisotropy measured during repeated trials of shearing at particular rates. Most of the error bars are small, demonstrating that a unique orientation state may be reproducibly achieved at each shear rate. As expected from the scattering patterns (Fig. 1), anisotropy increases with increasing shear rate. At low shear rates, in the yielding regime, the clay particles exhibit nearly random orientation, and high degree of misalignment away from the flow direction ($\chi = 30°$). As shear rate increases the particles become increasingly oriented towards the flow direction (χ drops below 10°) while anisotropy factor increases substantially. Based on the estimate of rotational diffusivity given above, the Peclet number $\left(Pe = \dot{\gamma}/D_r\right)$ varies from 3 to 3×10^4 over

the shear rate range covered in Fig. 4; it is hence not surprising to see these types of changes in the degree and direction of particle orientation. Under conditions of low *Pe*/low orientation, one normally would expect the orientation angle to approach a limiting value of 45° in shear flow. However, the presence of a particle network structure associated with yield stress behavior at low rates may affect particle dynamics to prevent this. There is excellent qualitative agreement between Fig. 4 and linear dichroism measurements of steady orientation in the 1–2 plane reported recently by Mobuchon et al. (2009a, b)—including the failure to reach 45° in the low shear rate orientation angle. Such agreement is remarkable given the wide disparity in length scales probed by X-ray and light scattering. Indeed, in light of differences found between X-ray and dichroism measurements of structural anisotropy upon flow cessation (see below), this agreement may well be somewhat fortuitous.

It is interesting to note the difference between our observation of significant alignment of individual clay particles, and the observations of Pignon et al. (1998) on aqueous clay dispersions. While Pignon et al. observed significant shear-induced alignment of larger-scale fractal network structures using light scattering under shear, SANS data collected at smaller length scales showed no evidence of flow-induced anisotropy at the single-particle level. However, their clay particles were much smaller, and dispersed in a much lower viscosity matrix, so that the single particle rotational diffusivity would be over seven orders of magnitude larger than in the present work; indeed, Pignon et al. concluded that shear was insufficient to overcome the dominance of Brownian motion in their experiments.

SAXS and WAXS measurements of anisotropy are broadly consistent with one another. However, there are certain quantitative differences. Anisotropy at lower shear rates is very similar for both SAXS and WAXS data. However, at higher shear rates (>1 s^{-1}), the anisotropy measured via SAXS is systematically lower than that measured via WAXS. Also, orientation angle data show small but systematic differences across all shear rates. There are a few possible reasons for these differences. First, the layered clay nanoparticles are polydisperse in size and shape. Within a polydisperse sample, different populations of particles will respond to flow differently. The polydispersity also means that some particles will have more silicate layers than others. The WAXS peak reflects Bragg diffraction from the layered structure of each clay particle. In particles consisting of relatively few layers, the Bragg diffraction will be more diffuse; as a result, larger particles with
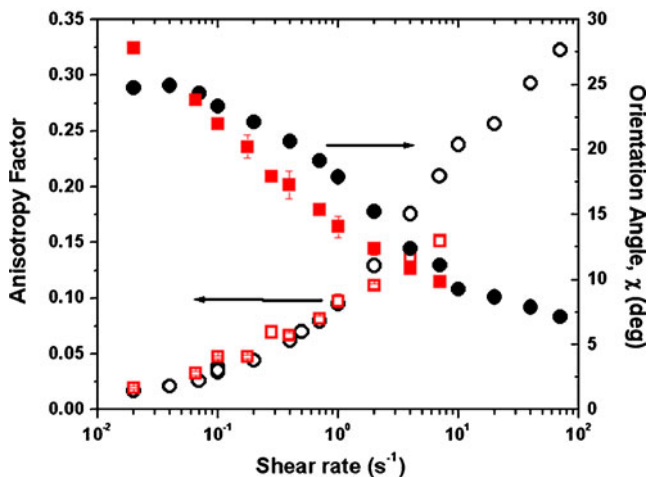

Fig. 4 Steady-state anisotropy factor (*open symbols*) and orientation angle (*closed symbols*) measured in the 1–2 plane as a function of shear rate for the 2 vol.% clay dispersion using SAXS (*unfilled squares*, *filled squares*) and WAXS (*unfilled circles*, *filled circles*)

a greater number of layers would be expected to have greater contribution to the WAXS scattering feature, and associated measurements of particle orientation. A second important difference in SAXS and WAXS is the length scale probed by the two techniques. Specifically, due to the larger length scale probed by SAXS, particle clustering due to interparticle interactions may affect the presumed relationship between the particle orientation distribution and anisotropic scattering in the SAXS regime. For very dilute suspensions with widely separated particles, SAXS should also report individual particle orientation. But in a more concentrated suspension, like the one studied here, anisotropic scattering from a cluster of several particles may lead to a SAXS pattern that differs from a simple superposition of anisotropic patterns from the constituent clay particles. Mobuchon et al. (2009a, b) have, in fact, observed shear rate-dependent states of aggregation in similar nonpolar dispersions via microscopic imaging. Conversely, the WAXS feature intrinsically probes the orientation at an individual particle level, and its fidelity in representing the particle orientation distribution should not be affected by the presence or absence of particle clusters. Such factors may contribute to the subtle differences seen in SAXS and WAXS results of Fig. 4. Their influence appears to be relatively minor in the case of steady shear flow; however, greater differences between SAXS and WAXS measurements of anisotropy are found in transient data described below.

Measurements of storage modulus following flow cessation provide evidence of structural evolution during relaxation similar to that reported by Mobuchon et al. (2007) (Fig. 5a). Throughout the relaxation process, the storage modulus is strongly dependent on the prior shear rate. For a low pre-shear rate the initial modulus is high, and changes relatively little during relaxation (studied here over an interval of 5,400 s). Conversely, when the pre-shear rate is high, the initial modulus is quite low, and increases substantially over the course of relaxation. However, even after extended relaxation, the final modulus after shearing at a high rate continues to be much lower than that found after shearing at a low rate. This strong dependence of structure on prior shear rate was investigated in detail by Mobuchon et al. (2007).

A common rheological motif in particulate suspensions is the emergence of a solid-like plateau modulus at low frequencies in oscillatory rheological testing (Raghavan and Khan 1995; Du et al. 2004), frequently attributed to the presence of a mechanically percolated particulate network (Krishnamoorti et al. 1996).
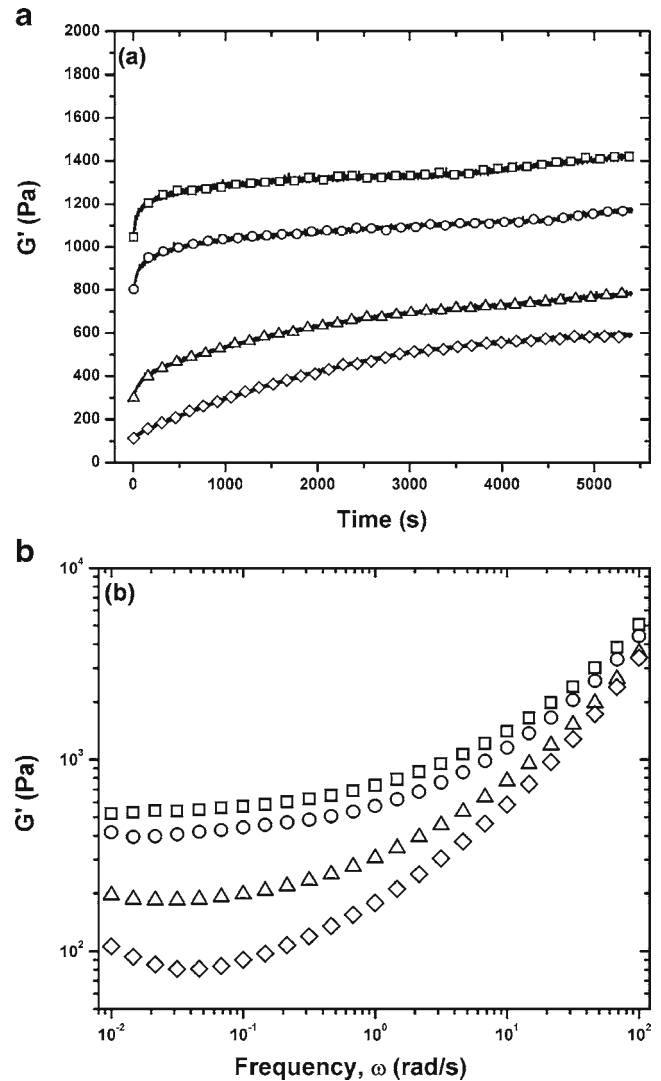
Fig. 5 a Storage modulus (measured at an angular frequency of 10 rad/s) measured as a function of time following cessation of steady shear flow. **b** Frequency sweep measured after steady shear flow and a rest time of 5,400 s. *Symbols* indicate the pre-shear rates: 0.02 (*unfilled squares*), 0.1 (*unfilled circles*), 1.0 (*unfilled triangles*), and 4.0 s^{-1} (*unfilled diamonds*)

Viscoelastic measurements on pre-sheared, then 're-laxed' samples again reveal the strong influence of pre-shear rate on the structural state of this clay suspension (Fig. 5b). If pre-sheared at a low rate, the sample exhibits a large low frequency modulus, indicating a well developed network microstructure of clay particles. Conversely, even after 5,400 s of relaxation, high pre-shear conditions result in a substantially softer structural state with lower modulus. These observations again closely resemble the behavior documented by Mobuchon et al. (2007) in a more highly concentrated dispersion. For higher pre-shear rates the modulus

appears to increase with decreasing frequency. This aphysical result is an experimental artifact, reflecting the fact that the structure, and hence dynamic modulus, continues to evolve at long times (Fig. 5a), even after 5,400 s of relaxation. The frequency sweeps in Fig. 5b were performed from high to low frequency; on the longer time scales required to collect low frequency data, the continued growth in G' leads to the apparently anomalous behavior.

The suspending matrix used here is Newtonian and, hence, does not contribute to the storage modulus. All changes in the elastic modulus observed in Fig. 5 are thus directly linked to evolution of the clay microstructure upon flow cessation. The pre-shear rate dependence of the initial G' indicates the degree of break down of the clay network like structure: shearing at higher rates disrupts the network more severely than shearing at low rates, within the 'yielding' regime. During rest, a particulate network can slowly reform, manifested by the gradual growth of G'; however, strong pre-shear rate dependence in network structure apparently exists even after prolonged relaxation. Given that the clay particles in the suspension studied here are Brownian, one expects rotational diffusion to play a role in this structural evolution.

Direct measurements of the clay orientation state confirm a strong influence of shear history on the suspension microstructure following flow cessation (Fig. 6; orientation angle data, not presented here, shows negligible change over the course of relaxation). As anticipated by the steady shear data, the initial anisotropy increases with increasing pre-shear rate. A loss of anisotropy during the relaxation period provides direct evidence of Brownian rotation of the clay particles in this suspension; indeed, the time scale of this relaxation is consistent with estimates of rotational diffusivity given above. In every respect, there are close parallels between the orientation data of Fig. 6 and the mechanical data of Fig. 5a. The high anisotropy factor observed at short time and high rates correlates to the suppressed elastic modulus. Relaxation of the induced anisotropy parallels the corresponding growth in G'; in particular, large changes in both modulus and anisotropy are observed for high pre-shear rates, while only small changes are observed in both orientation and modulus during relaxation from low pre-shear rates. Finally, as found in the mechanical response, the structural state is observed to be pre-shear rate dependent even after prolonged relaxation: when sheared at high rates, only a partial decay in anisotropy is observed.

In the nanocomposite literature, changes in dynamic modulus following flow cessation are often in-
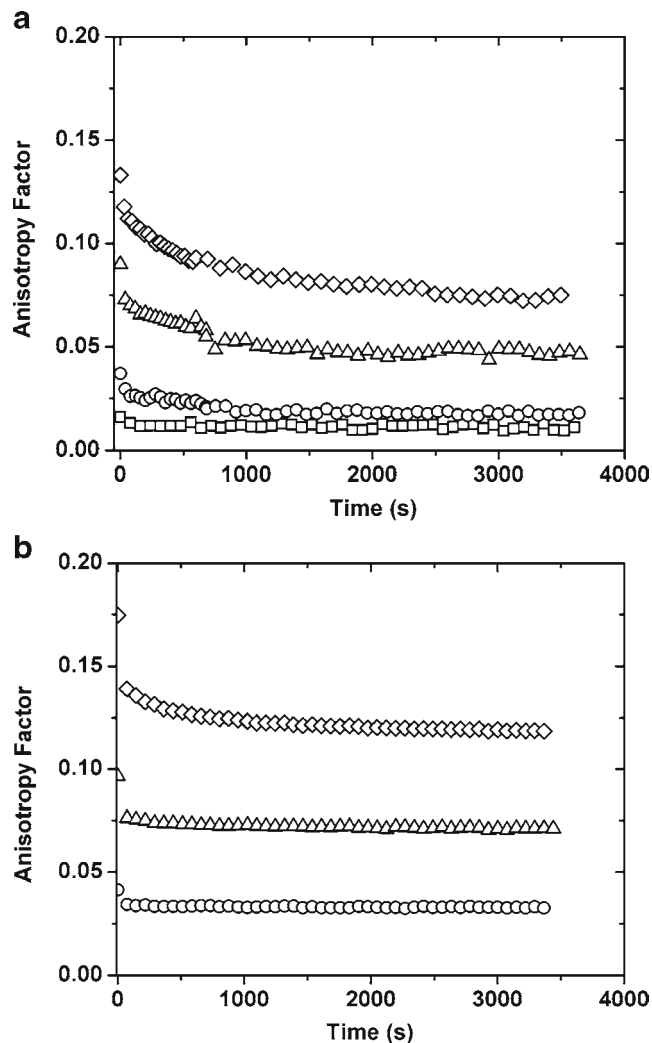
Fig. 6 Anisotropy factor measured using **a** SAXS and **b** WAXS, following cessation of steady shear flow at rates of 0.02 (*unfilled squares*), 0.1 (*unfilled circles*), 1.0 (*unfilled triangles*), and 4.0 s^{-1} (*unfilled diamonds*)

terpreted in terms of two different microstructural features: either as a direct manifestation of changes in the orientation distribution of the dispersed particles (Krishnamoorti et al. 1996; Krishnamoorti and Yurekli 2001; Letwimolnun et al. 2007), or in the context of reformation of a percolated nanoparticle network. In the present case, we hypothesize that these different structural features are strongly coupled. Shearing at high rates both induces particle orientation and disrupts the particle network, leading to suppressed dynamic modulus. During relaxation, Brownian motion both facilitates network reformation and leads to loss of particle orientation. At the same time, the redevelopment of a particle network "freezes" the dispersion in a nonequilibrium state, in which particles are unable

to continue to relax towards isotropy. It is well known that percolation in networks of anisotropic particles is highly dependent on the degree of particle orientation, and that lower degrees of percolation result from higher levels of orientation (Du et al. 2004, 2005). During relaxation from a high pre-shear rate, orientation relaxation is halted in a condition of high particle orientation, which limits the extent of possible network reformation. It is important to note that this picture need not be universal. In more highly concentrated clay dispersions (formulated differently than the sample studied here), we have found that evolution of dynamic modulus may be highly decoupled from particle orientation (Dykes et al. 2010). As mentioned earlier, Letwimolnun et al. (2007) have attempted to model network structure and orientation dynamics in polymer/clay nanocomposites, but the two structural features were treated independently. Possible coupling between evolution and network structure and orientation suggested in Figs. 5 and 6 may require a more general modeling approach in which evolution of these structural characteristics is interdependent.

It is interesting to note that linear dichroism measurements of structural anisotropy in similar dispersions showed no relaxation upon flow cessation (Mobuchon et al. 2009a, b). To explain this difference, we suggest that it is likely that dichroism—whose origin is anisotropic light scattering—is more sensitive to the larger length-scale anisotropic cluster structures that have been observed following shear via direct real-space imaging using optical microscopy (Mobuchon et al. 2009b), rather than directly measuring orientation at the level of individual clay particles. The lack of any significant structural relaxation at such larger length scales is to be expected.

During relaxation, SAXS (Fig. 6a) and WAXS (Fig. 6b) data reveal qualitatively similar phenomena. Both sets of data show more relaxation of induced anisotropy following high pre-shear rates, and little relaxation of anisotropy following low pre-shear rates. However, there are some noteworthy differences between SAXS and WAXS data. First, the WAXS data do not show as much relaxation as the SAXS data; the final orientation state measured by WAXS is systematically higher. As noted earlier, we expect larger particles (i.e. those with a greater number of silicate layers) to contribute disproportionately to the WAXS scattering. However, such larger particles would relax more slowly than the average, and perhaps be locked into a redeveloping network structure more rapidly, limiting their ultimate degree of relaxation. Another interesting distinction is found at very short times, where the WAXS measurements of orientation show a more

rapid initial drop in anisotropy than the SAXS data. The origin of this effect is not clear.

Flow reversal experiments are an effective way to study orientation dynamics under conditions in which the shear rate magnitude—hence, the degree of any persistent network like structure—is held constant. The mechanical response to flow reversal is straightforward (Fig. 7). The steady state stress, which increases monotonically with increasing shear rate, changes sign when the direction of flow is reversed, and returns to its steady state value within ∼5 strain units. While reversals with intermediate periods of relaxation can show significant stress overshoots (Solomon et al. 2001; Mobuchon et al. 2007; Letwimolnun et al. 2007), no overshoots are seen in Fig. 7. In the absence of rest time, there is no opportunity for the network reformation believed to be responsible for stress overshoots (Solomon et al. 2001; Mobuchon et al. 2007; Letwimolnun et al. 2007). Using either SAXS or WAXS, the anisotropy factor shows a transient dip in anisotropy when flow is reversed (Figs. 8a and 9a). The drop in anisotropy can be attributed to a more isotropic intermediate clay orientation state, as particles reorient towards the new flow direction. The steady state anisotropy is reestablished in less than 10 strain units. The reorientation of particles is directly manifested in orientation angle data, which show a rapid change in sign following flow reversal (Figs. 8b and 9b). After steady state is achieved (again within ∼10 strain units), the magnitude of the orientation angle in the reversed direction is the same as prior to reversal, showing that
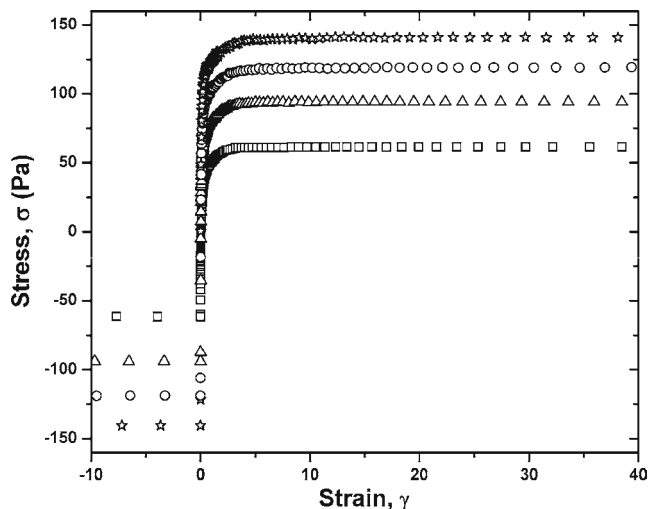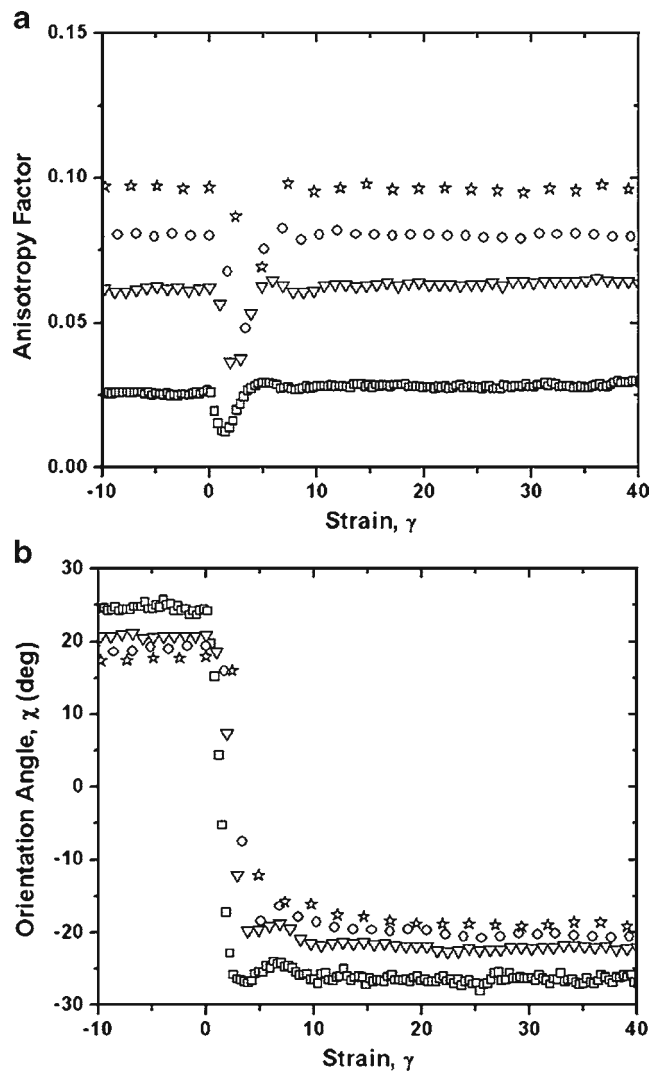

Fig. 7 Shear stress measured as a function of strain following flow reversal at shear rates of 0.07 (*unfilled squares*), 0.4 (*unfilled triangles*), 0.7 (*unfilled circles*), and 1.0 s^{-1} (*asterisk*)
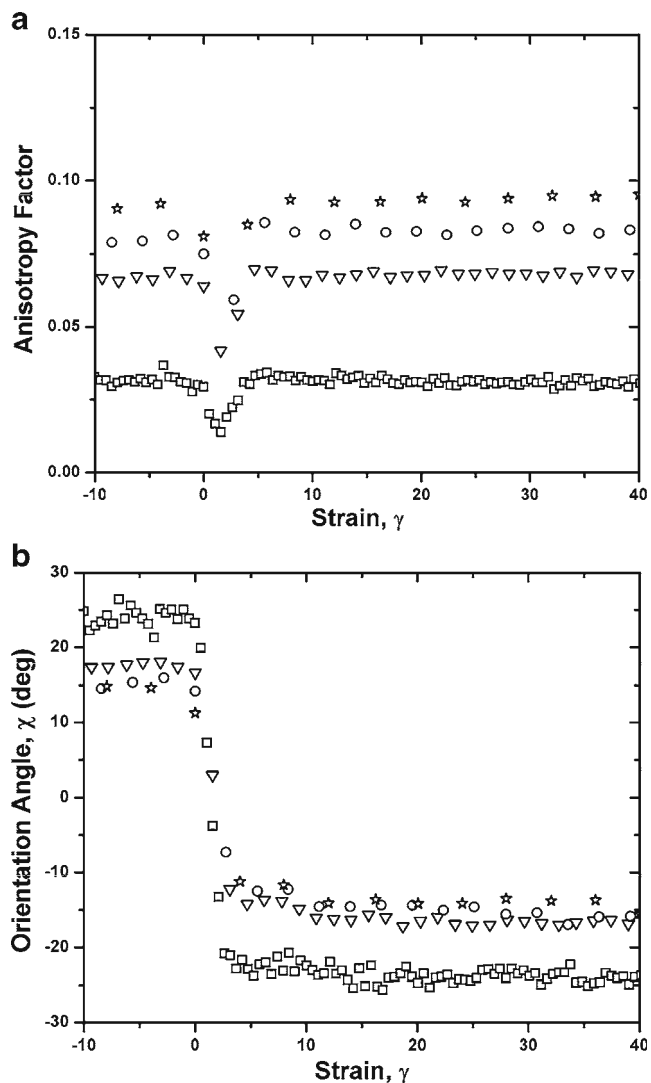
Fig. 8 **a** Anisotropy factor and **b** orientation angle measured using SAXS as a function of shear strain following flow reversal at shear rates of 0.07 (*unfilled squares*), 0.4 (*unfilled triangles*), 0.7 (*unfilled circles*), and 1.0 s^{-1} (*asterisk*)

Fig. 9 **a** Anisotropy factor and **b** orientation angle measured using WAXS as a function of strain following flow reversal at shear rates of 0.07 (*unfilled squares*), 0.4 (*unfilled triangles*), 0.7 (*unfilled circles*), and 1.0 s^{-1} (*asterisk*)

the same structural state is achieved upon reversal, but in the opposite direction.

Both SAXS and (especially) WAXS reversal data show clear evidence of oscillations in the transient response of both anisotropy and orientation angle. The orientation dynamics of isolated anisotropic particles dispersed in Newtonian fluids follow periodic trajectories solved by Jeffery (1922) that provide a natural explanation for oscillations transient flows. Even in the concentrated dispersion studied here, it is reasonable to expect that the fundamental hydrodynamics of disk-like particles may be manifested in these structural oscillations. Note that the oscillations in Fig. 9 scale with shear strain, as would be expected for Jeffery orbit dynamics. The fact that the oscillatory character of the transient

response is more clearly manifested in WAXS data may, again, reflect the fact that WAXS measurements may be biased in favor of larger/thicker particles, and hence be dominated by a subset of particles that exhibit more homogeneous orientation dynamics.

Unlike the case of shear reversal, experiments involving a step down in shear rate should involve both time-dependent changes in the particle orientation as well the extent of a particle network. Mobuchon et al. (2007) observed striking stress undershoots following step down in shear rate, which are also found in the current sample (Fig. 10a). The magnitude of the stress undershoot is strongly dependent on the magnitude of step shear applied. Step down to a final shear rate of 0.02 s^{-1} from an initial shear rate of 7 s^{-1} causes a

11
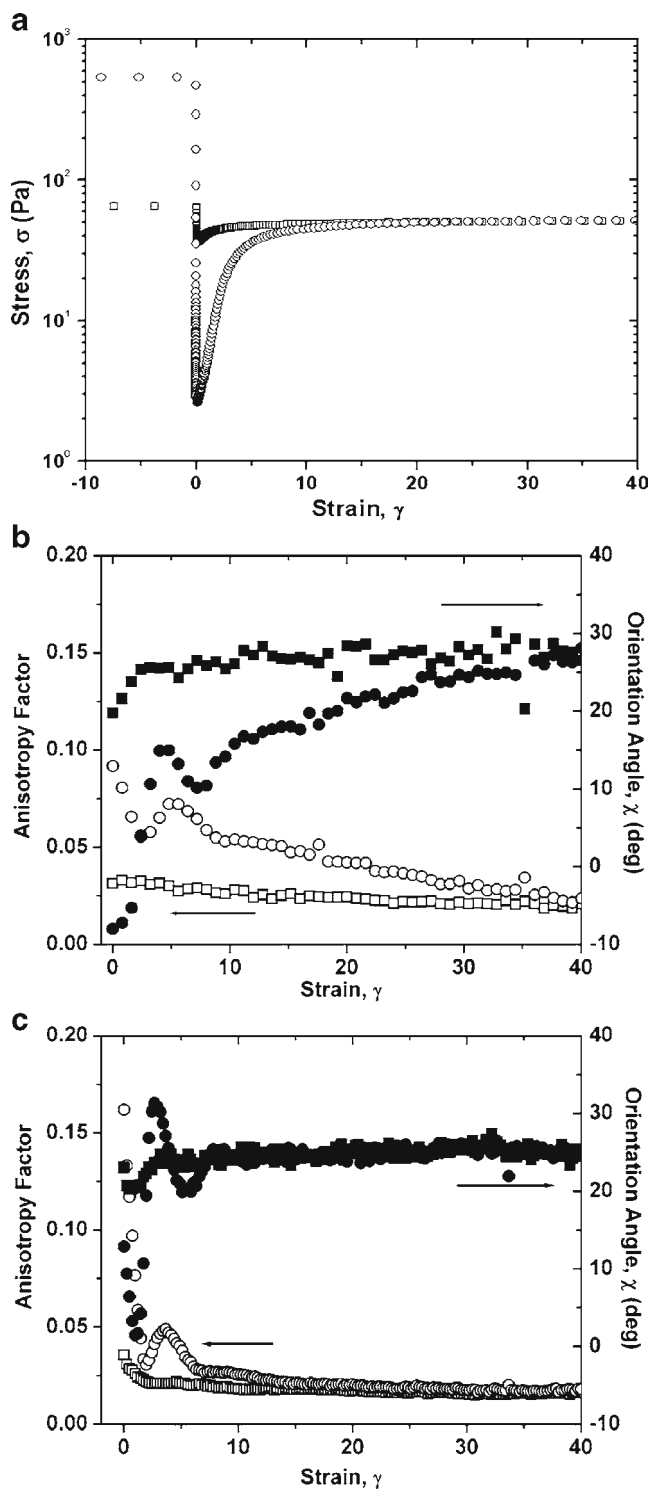
Fig. 10 Mechanical and structural response to step down experiments. **a** Shear stress measured as a function of strain following step down to a final shear rate 0.02 s⁻¹. **b** SAXS and **c** WAXS measurements of anisotropy factor (*open symbols*) and orientation angle (*closed symbols*) as a function of strain following step down to a final shear rate of 0.02 s⁻¹. *Symbols* designate initial shear rates: 0.1 (*unfilled squares*) and 7.0 s⁻¹ (*unfilled circles*)

much larger undershoot than from an initial shear rate of 0.1 s⁻¹ (note the log scale on stress in Fig. 10a). Following step down, the shear stress approaches a reproducible steady state value within ∼20 strain units. Relative to transients observed in reversal, SAXS data show a much more gradual evolution of anisotropy and orientation angle toward their new steady state values, particularly for the larger step from 7 to 0.02 s⁻¹ (Fig. 10b). For this larger step, pronounced oscillations in both anisotropy and orientation angle are superimposed on the transition between the steady state values representative of the initial and final shear rates. For the smaller step, in which the degree of orientation is already low to start, the transient orientation dynamics are more subdued. WAXS data (Fig. 10c) reveal similar phenomena as the SAXS data, notably pronounced oscillations in anisotropy and orientation angle following the larger step down. There is, however, a notable discrepancy between SAXS and WAXS data for the orientation angle dynamics for this particular protocol. Since this step down experiment may involve changes in both the orientation state and the degree of clustering of the constituent clay particles, it is difficult to propose possible origins for this difference.

Unlike the case of flow cessation, there appears to be little direct correlation between the transient mechanical and orientation response in this step down experiment. For the larger step down, the mechanical response exhibits a stress undershoot of about 1.5 orders of magnitude. While interesting structural dynamics are observed, neither SAXS nor WAXS measurements show changes dramatic enough to explain this observation. Rather, it is likely that the transient undershoot reflects changes in the particle network structure; such structural changes might be more clearly manifested in light scattering or dichroism experiments which probe larger length scales (Mobuchon et al. 2009a, b). Steady-state viscosity measurements (Fig. 3) suggest that any particle network would be largely disrupted at shear rate of 7 s⁻¹, where the viscosity is not that much larger than that of the viscous polymer matrix. Immediately upon step down, the sample initially retains this low viscosity, and the stress drops dramatically. Continued shearing, however, leads to reformation of a particle network, and, accordingly, the dramatic increase in viscosity expected from Fig. 3. Conversely, in this same experiment, SAXS and WAXS both show dramatic structural oscillations that have no obvious manifestations in the mechanical response. As in the case of flow reversal, such oscillations are likely due to Jeffery like tumbling motion of the clay particles. The comparative strength of the oscillatory response relative to that found in reversal may reflect the fact

that pre-shearing at a high initial rate substantially breaks up particle network/cluster structures, allowing particles—initially—greater latitude to rotate in the shear flow. The comparatively slow approach to steady state in anisotropy factor and orientation angle may be due to hindrance from the developing particle network. All of these characteristics are considerably muted in the smaller step down experiment (0.1 to $0.02\,\mathrm{s}^{-1}$), since a much more robust particle network is likely already present during the pre-shearing at this lower rate.

Conclusions

Direct X-ray scattering measurements of particle orientation during steady and transient shear flows in this model polymer/clay nanocomposite provide useful insights into the microscopic origins of the observed rheological behavior. In the low rate, yield-stress regime, there is negligible orientation of clay particles within the 1–2 plane. Increasing shear rate (and hence Peclet number) leads to increased particle alignment, and rotation of the average orientation direction towards the flow direction. Upon flow cessation, partial relaxation of orientation is observed, that correlates extremely closely to evolution of dynamic moduli. Even after prolonged relaxation, the structural state of the sample depends on the prior shear conditions. The orientation state responds quite rapidly to shear flow reversal, and although the structural data show hints of oscillatory Jeffery orbit dynamics, the bulk mechanical response is rather featureless. Conversely, the shear stress shows remarkable undershoots upon step-down in shear rate of large magnitude. There is no obvious explanation for this phenomenon in the observed orientation dynamics at nano scale; rather, this thixotropic behavior is attributed to the reformation of a particle network structure that had been disrupted by the prior shearing at high rates. Orientation measurements derived from small- and wide-angle X-ray scattering generally provide consistent pictures of the steady and transient orientation state, although there are quantitative differences due to the different length scales probed by the two methods.

References

Alexandre M, Dubois P (2000) Polymer-layered silicate nanocomposites: preparation, properties and uses of a new class of materials. Mater Sci Eng R Rep 28:1–63

Aubry T, Razafinimaro T, Médéric P (2005) Rheological investigation of the melt state elastic and yield properties of a polyamide-12 layered silicate nanocomposite. J Rheol 49:425–440

Bafna A, Beaucage G, Mirabella F, Mehta S (2003) 3D Hierarchical orientation in polymer-clay nanocomposite films. Polymer 44:1103–1115

Balazs AC (2003) Predicting the morphology of nanostructured composites. Curr Opin Solid St M 7:27–33

Camerel F, Gabriel JCP, Batail P, Panine P, Davidson P (2003) Combined SAXS-rheological studies of liquid-crystalline colloidal dispersions of mineral particles. Langmuir 19:10028–10035

Caputo FE, Burghardt WR (2001) Real-time 1–2 plane SAXS measurements of molecular orientation in sheared liquid crystalline polymers. Macromolecules 34:6684–6694

Caputo FE, Burghardt WR, Krishnan K, Bates FS, Lodge TP (2002) Time-resolved small-angle x-ray scattering measurements of a polymer bicontinuous microemulsion structure factor under shear. Phys Rev E 66:041401

Du F, Scogna RC, Zhou W, Brand S, Fischer JE, Winey KI (2004) Nanotube networks in polymer nanocomposites: rheology and electrical conductivity. Macromolecules 37:9048–9055

Du F, Fischer JE, Winey KI (2005) Effect of nanotube alignment on percolation conductivity in carbon nanotube/polymer composites. Phys Rev B 72:121404

Dykes LMC, Torkelson JM, Burghardt WR, Krishnamoorti R (2010) Shear-induced orientation in polymer/clay dispersions via in situ X-ray scattering. Polymer 51:4916–4927. doi:10.1016/j.polymer.2010.08.013

Fornes TD, Yoon PJ, Keskkula H, Paul DR (2001) Nylon 6 nanocomposites: the effect of matrix molecular weight. Polymer 42:9929–9940

Galgali G, Ramesh C, Lele A (2001) A rheological study on the kinetics of hybrid formation in polypropylene nanocomposites. Macromolecules 34:852–858

Galgali G, Agarwal S, Lele A (2004) Effect of clay orientation on the tensile modulus of polypropylene-nanoclay composites. Polymer 45:6059–6069

Giannelis EP (1996) Polymer layered silicate nanocomposites. Adv Mater 8:29–35

Giannelis EP, Krishnamoorti R, Manias E (1999) Polymer-silicate nanocomposites: model systems for confined polymers and polymer brushes. Adv Polym Sci 138:107–147

Guinier A, Fournet G (1955) Small-angle scattering of x-rays. Wiley, New York

Jeffery GB (1922) The motion of ellipsoidal particles immersed in a viscous fluid. P Roy Soc A 102:161–179

Kojima Y, Fukumori K, Usuki A, Okada A, Kurauchi T (1993) Gas permeabilities in rubber clay hybrid. J Mater Sci Lett 12:889–890

Koo CM, Kim MJ, Choi MH, Kim SO, Chung IJ (2003) Mechanical and rheological properties of the maleated polypropylene-layered silicate nanocomposites with different morphology. J Appl Polym Sci 88:1526–1535

Krishnamoorti R, Yurekli K (2001) Rheology of polymer layered silicate nanocomposites. Curr Opin Colloid In 6:464–470

Krishnamoorti R, Vaia RA, Giannelis EP (1996) Structure and dynamics of polymer-layered silicate nanocomposites. Chem Mater 471:1728–1734

Lele A, Mackley M, Galgali G, Ramesh C (2002) In situ rheo-x-ray investigation of flow-induced orientation in layered silicate-syndiotactic polypropylene nanocomposite melt. J Rheol 46:1091–1110

Letwimolnun W, Vergnes B, Ausias G, Carreau PJ (2007) Stress overshoots of organoclay nanocomposites in transient shear flow. J Non-Newton Fluid Mech 141:167–179

Lim YT, Park OO (2001) Phase morphology and rheological behavior of polymer/layered silicate nanocomposites. Rheol Acta 40:220–229

Medellin-Rodriguez FJ, Burger C, Hsiao BS, Chu B, Vaia R, Phillips S (2001) Time-resolved shear behavior of end-tethered Nylon 6-clay nanocomposites followed by non-isothermal crystallization. Polymer 42:9015–9023

Mobuchon C, Carreau PJ, Heuzey M-C (2007) Effects of flow history on the structure of a non-polar polymer/clay nanocomposite model system. Rheol Acta 46:1045–1056

Mobuchon C, Carreau PJ, Heuzey M-C, Reddy NK, Vermant J (2009a) Anisotropy of nonaqueous layered silicate suspensions subjected to shear flow. J Rheol 53:517–538

Mobuchon C, Carreau PJ, Heuzey M-C (2009b) Structural analysis of non-aqueous layered silicate suspensions subjected to shear flow. J Rheol 53:1025–1048

Nam PH, Maiti P, Okamoto M, Kotaka T, Hasegawa N, Usuki A (2001) A hierarchical structure and properties of intercalated polypropylene/clay nanocomposites. Polymer 42:9633–9640

Okada A, Kawasumi M, Kurauchi T, Kamigaito O (1987) Synthesis and characterization of a nylon 6-clay hybrid. Polymer Preprints 28:447–448

Pignon F, Magnin A, Piau J-M, Cabane B, Lindner P, Diat O (1997) Yield stress thixotropic clay suspension: investigations of structure by light, neutron and x-ray scattering. Phys Rev E 56:3281–3289

Pignon F, Magnin A, Piau J-M (1998) Thixotropic behavior of clay dispersions: combinations of scattering and rheometric techniques. J Rheol 42:1349–1373

Pujari S, Rahatekar SS, Gilman JW, Koziol KK, Windle AH, Burghardt WR (2009) Orientation dynamics in multi-wall carbon nanotube dispersions under shear flow. J Chem Phys 130:214903

Raghavan SR, Khan SA (1995) Shear-induced microstructural changes in flocculated suspensions of fumed silica. J Rheol 39:1311–1325

Ren JX, Krishnamoorti R (2003) Nonlinear viscoelastic properties of layered-silicate-based intercalated nanocomposites. Macromolecules 36:4443–4451

Salem AJ, Fuller GG (1985) Small angle light scattering as a probe of flow-induced particle orientation. J Colloid Interface Sci 108:149–157

Schaeffer DW, Justice RS (2007) How nano are nanocomposites? Macromolecules 40:8501–8517

Solomon MJ, Almusallam AS, Seefeldt KF, Somwangthanaroj A, Varadan P (2001) Rheology of polypropylene/clay hybrid materials. Macromolecules 34:1864–1872

Varlot K, Reynaud E, Kloppfer MH, Vigier G, Varlet J (2001) Clay-reinforced polyamide: preferential orientation of the montmorillonite sheets and the polyamide crystalline lamellae. J Polym Sci B Polym Phys 39:1360–1370

Vermant J, Ceccia S, Dolgovskij MK, Maffettone PL, Macosko CW (2007) Quantifying dispersion of layered nanocomposites via melt rheology. J Rheol 51:429–450

Xu L, Reeder S, Thopasridharan M, Ren JX, Shipp DA, Krishnamoorti R (2005) Structure and melt rheology of polystyrene-based layered silicate nanocomposites. Nanotechnology 16:S514-S521